Journal of Thermal Analysis and Calorimetry, Vol. 90 (2007) 3, 755–760

XRD, TEM AND THERMAL ANALYSIS OF Fe DOPED BOEHMITE NANOFIBRES AND NANOSHEETS

*Y. Zhao, R. L. Frost**, *W. N. Martens and H. Y. Zhu*

Inorganic Materials Research Program, School of Physical and Chemical Sciences, Queensland University of Technology, GPO Box 2434, Brisbane Queensland 4001, Australia

Iron doped boehmite nanofibres with varying iron content have been prepared at low temperatures using a hydrothermal treatment in the presence of poly(ethylene oxide) surfactant. The resultant nanofibres were characterized by X-ray diffraction (XRD), and transmission electron microscopy (TEM). TEM images showed the resulting nanostructures are predominantly nanofibres when Fe doping is no more than 5%; in contrast nanosheets were formed if Fe doping was above 5%. For the 10% Fe doped boehmite, a mixed morphology of nanofibres and nanosheets were obtained. Nanotubes instead of nanofibres were observed in samples with 20% added iron. The Fe doped boehmite and the subsequent nanofibres/nanotubes were analysed by thermogravimetric and differential thermogravimetric methods. Boehmite nanofibres decompose at higher temperatures than non-hydrothermally treated boehmite and nano-sheets decompose at lower temperatures than the nanofibres.

Keywords: *acicular, boehmite, nanofibre, nanosheets, nanotube*

Introduction

Recently, synthesis of inorganic nanoscale materials with special properties have been of great interest in material science [1, 2], because their intrinsic properties of nanoscale materials are mainly determined by their composition, structure, crystallinity, size and morphology [3]. In particular, one dimensional (1D) nanoscale inorganic materials including nanofibers, nanowires and nanotubes have attracted intensive interest due to their distinctive geometries, novel physical and chemical properties and potential applications in numerous areas [4].

Because of its high surface area, chemical and thermally stable properties and mesoporous properties, alumina has been extensively used as carrier and support for a variety of industrial catalysts at high temperature as well as low temperature. Alumina can be employed as catalyst [5], adsorbent [6, 7], composite materials [8, 9] and ceramics [10–12]. Boehmite (γ-AlOOH), a principal oxo hydroxide of aluminium, is a crucial precursor in sol–gel technique for preparing high-purity and high-strength monolithic α-alumina ceramics for use as substrates for electronic circuits, abrasive grains, high-temperature refractory materials, fibres and thin films [13]. Boehmite nanofibres were first synthesised by Bugosh [14] in 1961. Nanofibres can be used as molecular building units in the preparation of core/shell materials [10, 15]. Also, since the resulting alumina prepared from boehmite can keep the original size and morphology after calcination, great effort has been devoted to the investigation of nanoscale boehmite materials, especially 1D nanostructures, such as nanofibres and nanotubes [16, 17].

Latterly, Zhu *et al.* [18] reported an interesting new synthesis method by using a surfactant. Rather than acting as templates as for the synthesis of mesoporous materials, the surfactant was able to direct formation of boehmite fibres [17]. It was also reported that a much higher Al concentration and lower temperatures can be used compared to traditional methods for the synthesis of boehmite nanofibres. This is an efficient approach of producing nanofibres in large quantity. The growth of boehmite nanofibres can be improved by a regular interval supply of fresh precipitate of aluminium hydrate and the fibres can grow to over 100 nm long when reaction conditions are well-controlled. It is well known that the necessity of later catalyst or absorbent separation is an important issue in industrial catalytic process and water treatment. Except for filtration technique, magnetic separation is another good method [19, 20]. To achieve magnetic property, doping with iron would be an ideal way. Besides, doped with iron, the resulting boehmite nanostructure may have special optical properties which will enable it to further industrial applications.

Thermal analysis has proved most useful for the analysis of minerals and related materials [21–30]. In this work, boehmite nanofibres based on Zhu's methodology were synthesised by introducing iron as dop-

* Author for correspondence: r.frost@qut.edu.au

1388–6150/$20.00
© 2007 Akadémiai Kiadó, Budapest
Akadémiai Kiadó, Budapest, Hungary
Springer, Dordrecht, The Netherlands

ant and a series of iron doped boehmite nanofibres with varying iron content have been systematically studied using thermogravimetric techniques.

Experimental

Synthesis of Fe-doped boehmite nanofibres

The detailed experimental procedure is as follows. A total amount of 0.25 mol aluminium nitrate and ferric nitrate were mixed before being dissolved in ultra-pure water. To make a comparison, mixtures with iron molar percentage of 0, 1, 2, 3, 4, 5, 10 and 20% were prepared separately and then dissolved in ultra-pure water to form a solution with a metal ion to H_2O molar ratio of 1:100 and heated to 80°C. 5 mol L^{-1} NaOH solution was then added dropwise at a constant rate of 5 mL min^{-1} to form precipitate. After that it was aged for three hours with constant stirring at 80°C, the resulting precipitate was recovered by centrifugation, washed with pure water four times to remove sodium nitrate. The fresh precipitate was then split into five parts evenly for hydrothermal treatment and characterization. Water and non-ionic PEO surfactant Tergitol 15-S-7 ($C_{12-14}H_{25-29}O(CH_2CH_2O)_7H$, Aldrich) with average molecular mass of ~508 were mixed with the first part of precipitate at a metal:PEO:H_2O molar ratio of 1:0.4:16. The viscous mixture is stirred for 1 h at room temperature and then transferred into an autoclave and kept in oven at 120°C. The remaining three parts of fresh precipitate and the same amount of ultra-pure water were added into autoclave every two days. Accordingly, the molar ratio of metal:PEO:H_2O changed to 2:0.4:32, 3:0.4:48 and 4:0.4:64, respectively, after 2, 4, 6 days. The final product was washed by water first and then acetone and dried in air at 80°C.

Methods

X-ray diffraction

XRD analyses were performed on a PANalytical X'Pert PRO X-ray diffractometer (radius: 240.0 mm). Incident X-ray radiation was produced from a line focused PW3373/10 Cu X-ray tube, operating at 45 kV and 35 mA, wavelength of 1.540596 Å. The incident beam passed through a 0.04 rad, Soller slit, a 1/2° divergence slit, a 15 mm fixed mask and a 1° fixed anti-scatter slit. After interaction with the sample, the diffracted beam was detected by an X'Celerator RTMS detector. The detector was set in scanning mode, with an active length of 2.022 mm. Samples were analysed utilising Bragg–Brentano geometry over a range of 3–75° 2θ with a step size of 0.02° 2θ, with each step measured for 200 s.

TEM analysis

A Philips CM 200 transmission electron microscopy (TEM) at 200 kV was used to investigate the morphology of the boehmite nanofibres. All samples were dispersed in absolute ethanol solution and then dropped on copper grids coated with carbon film, dried in an oven at 60°C for 10 min for TEM studies.

Thermal analysis

Thermal decomposition of the Fe-doped boehmite was carried out in a TA® Instruments incorporated high-resolution thermogravimetric analyzer (series Q500) in a flowing nitrogen atmosphere (60 cm^3 min^{-1}). Approximately 35 mg of each sample underwent thermal analysis, with a heating rate of 5°C min^{-1}, with resolution of 6 from 25 to 1000°C. With the isothermal, isobaric heating program of the instrument the furnace temperature was regulated precisely to provide a uniform rate of decomposition in the main decomposition stage.

Results and discussion

X-ray diffraction

The X-ray diffraction of the precipitated boehmite and the hydrothermally treated boehmite are shown in Figs 1a and b. The XRD patterns show the precipitates

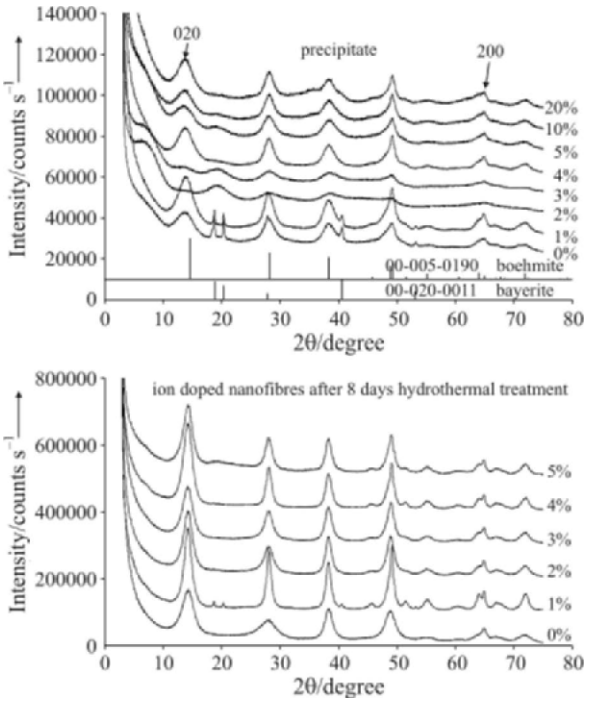

Fig. 1 a – Powder X-ray diffraction patterns of various % Fe doped boehmite and b – nanofibres

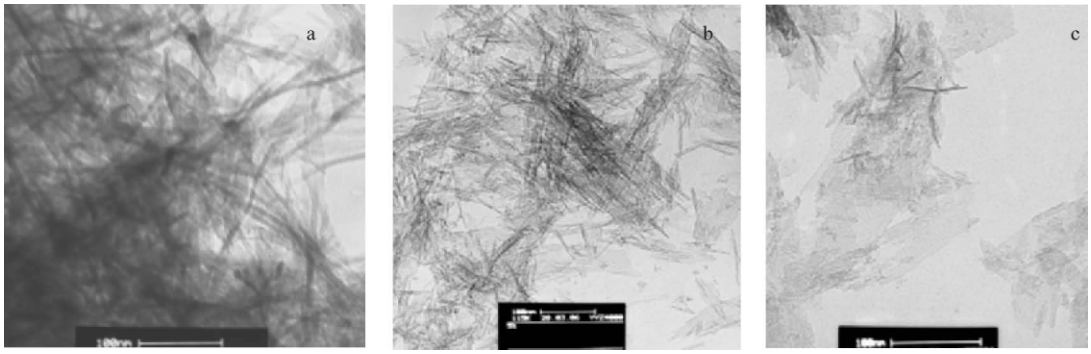

Fig. 2 TEM images of a – 3%, b – 5% and c– 10% Fe doped boehmite nanofibres

to be boehmite γ-AlOOH except for a minor amount of bayerite formed in 0 and 1% samples. By using the Debye–Scherrer equation the crystallite sizes vary initial from 15.5 nm in pure boehmite precipitates, to a constant value of ~22 nm with Fe doping. The XRD peaks in the patterns for 1% Fe doped boehmite nanostructures show decreased peak width with the increase in hydrothermal time, indicating a gradual increase in crystallinity of the nano-structures during the soft chemical treatment. The bayerite phase converts into boehmite with hydrothermal treatment.

Transmission electron microscopy

Typical transmission electron microscopy images for 3, 5 and 10% Fe doped nanofibres and nanosheets are shown in Figs 2a–c. The growth of pure boehmite nanofibres at 100°C has been systematically studied by Zhu *et al.* [17, 18, 31]. The average length of boehmite nanofibres after 8 days hydrothermal treatment was found to be ~92 nm. Hydrothermal treatment at 150°C resulted in the formation of 6 nm wide and 30 to 70 nm long lath like nanostructures [31]. In this work, boehmite nanostructures at 120°C were grown. As can be seen from Fig. 1a pure boehmite nanofibres with length up to 300 nm were synthesised, which is around three times long as that reported in a previous study [17].

As for iron doped samples, nanofibres were formed in samples with added iron content up to 10%. The iron doped boehmite fibres were up to 250 nm long while their width varied. Significant amounts of nanosheets were formed in samples with added iron percentage above 5%. Interestingly, most of the nanosheets formed have bevelled ends. As the iron doping was increased, more sheets formed; in particular, nanosheets are dominant in 10 and 20% iron doped samples. The nanofibres in these two samples aggregated in a parallel fashion forming bundle-like nanostructures resulting from increased surface charge of the nanostructure with increasing amounts of Fe. No nanofibres were observed in the 20% iron doped sample; however, nanotubes of 40–100 nm in length and 5–10 nm in diameter were formed. The Fe content affects not only the growth of the nanofibres but also the aggregation of nanostructures. At low Fe content, nanofibres with regular shape were formed; at a higher iron content, nanofibres aggregated parallel resulting in the formation of nanosheets with pointed ends; at high Fe content, no fibres are formed and some of the sheets rolled to form nanotubes.

Thermogravimetric analysis

The thermogravimetric analysis and the differential thermal analysis of boehmite and Fe doped boehmite and their nanostructures with varying amounts of Fe from 0 to 20% are shown in Figs 3–5. The results of the

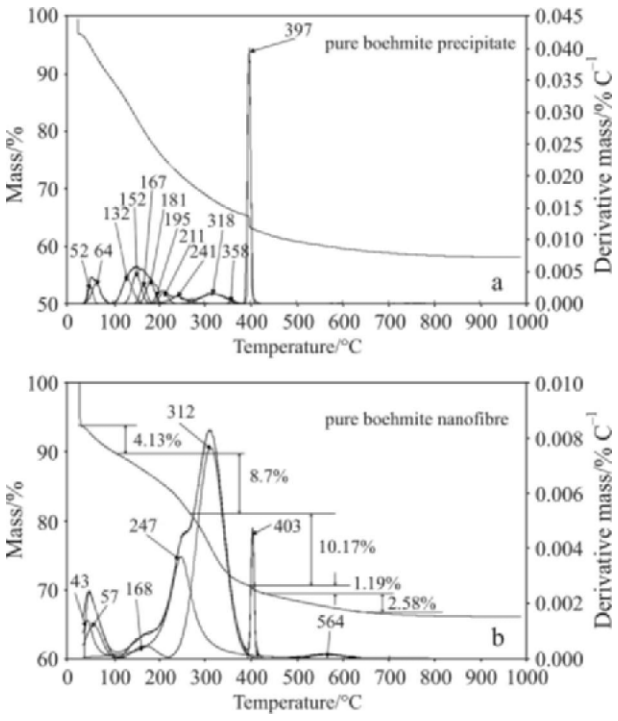

Fig. 3 Thermal analysis patterns of boehmite and boehmite nanofibres

thermal analyses are reported in Table 1, including the results form other Fe doped boehmite compositions.

Pure boehmite shows four decomposition steps . The step which is characteristic of boehmite is the sharp DTG step at 397°C with a mass loss of 4.55%. The first mass loss occurs at around 50°C with a mass loss of 8.11%. This mass loss step is attributed to adsorbed water. The second mass loss step is observed at around 152°C and accounts for the major mass loss step with 18.15% mass loss. This mass loss is attributed to interstitial water trapped between the boehmite layers. The theoretical mass loss based upon the equation:

$$2AlOOH \rightarrow Al_2O_3 + H_2O$$

is 11.5%. In order to synthesize the boehmite nanofibres, the boehmite (precipitate) is hydrothermally treated at 120°C for 8 days. In comparison the thermal analysis of the boehmite nanofibres (Fig. 3b) shows a large thermal decomposition step at 247 and 312°C with a mass loss of 18.87%. It is concluded that the boehmite nanofibres thermally decompose at a higher temperature than boehmite. The sharp band at 403°C is attributed to boehmite in a non-fibre form.

The 1% Fe doped boehmite thermal decomposition shows an additional sharp mass loss of 12.15% is observed at 195°C. This mass loss is attributed to the decomposition of goethite according to the equation:

$$2FeOOH \rightarrow Fe_2O_3 + H_2O$$

The boehmite precipitate decomposes over a temperature range from 229 to 364°C. In the 1% Fe doped boehmite nanofibre the peak at 207°C is diminished in intensity with a 1.49% mass loss. This decomposition is attributed to the combustion of the surfactant molecules used to template the nanofibres. The boehmite nanofibre decomposes over the 343 to 383°C. There is a 13.90% mass loss over this temperature range. It is concluded that boehmite nanofibres decompose at temperatures higher than for untreated boehmite.

For the 2% Fe doped boehmite four decomposition steps are observed at 50°C (7.25%), 169°C (14.21%), 302°C (11.44%) and 447°C (1.90%). These thermal decomposition steps are attributed to (a) the loss of adsorbed water, (b) the decomposition of the surfactant, (c) the thermal decomposition of the goethite, (d) the decomposition of boehmite. The thermal decomposition at temperatures above 400°C is attributed to impurities. Step (c) is different to that of this step observed for the 1% Fe doped boehmite. It is possible that the goethite is an Al substituted goethite [32–34]. For the 2% Fe doped boehmite nanofibres two decomposition steps are observed at 245 and 335°C with mass losses of 7.35 and 13.98%.

The thermal decomposition of the 3% Fe doped boehmite and 3% Fe doped boehmite nanofibres are similar to that of the 2% Fe doped materials. For the 3% Fe doped boehmite nanofibre two mass loss steps are observed at 289 and 340°C with mass losses of 10.55 and 8.44%. For the 4% Fe doped boehmite thermal decomposition takes place over a wide temperature range from 269 to 374°C. Such a wide temperature range is indicative of ill defined and even amor-

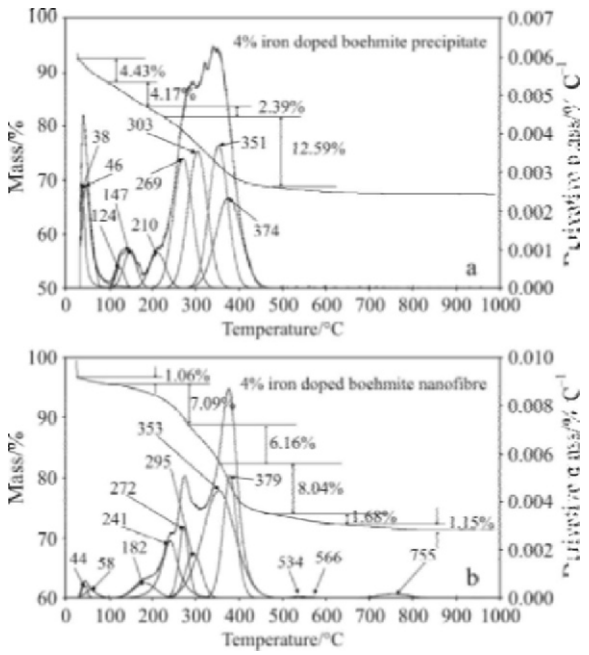

Fig. 4 Thermal analysis patterns of 4% Fe doped boehmite and boehmite nanofibres

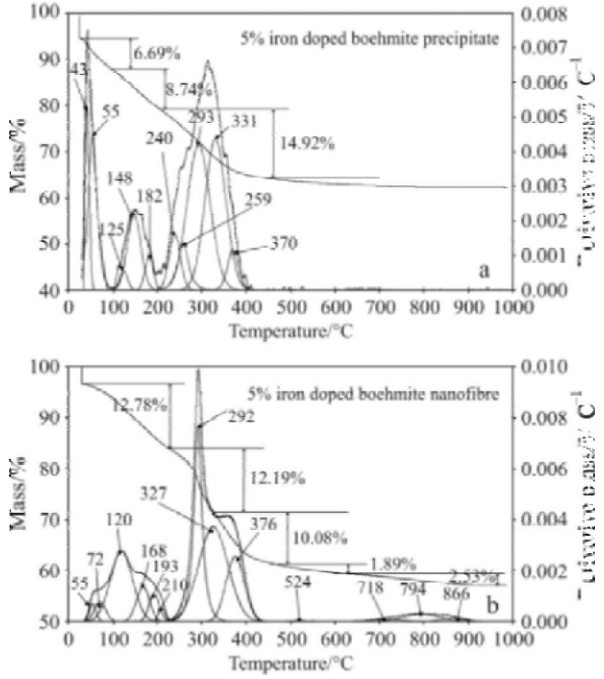

Fig. 5 Thermal analysis patterns of 5% Fe doped boehmite and boehmite nanofibres

Table 1 Results of the thermal analysis of boehmite and Fe doped boehmite and the equivalent nanofibres

Added Fe %		Decomposition step			
		First	Second	Third	Fourth
Precipitate	0	8.11%/55°C	18.15%/152°C	4.92%/318°C	4.55%/397°C
	1	7.34%/50°C	12.15%/195°C	25.52%/348°C	–
	2	7.25%/50°C	14.21%/169°C	11.44%/302°C	1.90%/447°C
	3	6.88%/55°C	11.51%/171°C	13.74%/313°C	1.91%/702°C
	4	4.43%/46°C	4.17%/147°C	14.98%/327°C	–
	5	6.69%/50°C	8.74%/148°C	14.92%/351°C	–
	10	6.20%/50°C	10.15%/139~250°C	10.43%/337°C	–
	20	3.96%/50°C	7.99%/143~268°C	7.73%/350°C	–
Nanofibre	0	4.13%/50°C	8.70%/247°C	10.17%/312°C	1.19%/403°C
	1*	1.78%/50°C	1.37%/213°C	14.42%/384°C	–
	1	1.30%/50°C	1.49%/207°C	13.90%/383°C	–
	2	1.82%/50°C	7.35%/245°C	13.98%/335°C	–
	3	1.78%/50°C	10.55%/289°C	8.44%/340°C	–
	4	1.06%/50°C	7.09%/272°C	6.16%/353°C	8.04%/379°C
	5	12.78%/120°C	12.19%/292°C	10.08%/376°C	
	10	1.00%/50°C	3.62%/230°C	4.04%/295°C	11.09%/376°C
	20	1.14%/50°C	–	–	17.40%/380°C

*hydrothermally treated for 6 days

phous boehmite materials (Figs 4a and b). The thermal decomposition at 241 and 272°C is attributed the combustion of the surfactant templating molecules. The temperature may be compared with the temperatures of 147 and 210°C for the 4% doped boehmite precipitate. For the 4% Fe doped boehmite nanofibres two decomposition steps at 272 and 379°C with mass losses of 7.09 and 14.20%. A similar set of results is observed for the 5% Fe doped boehmite precipitate and nanofibres. Three decomposition steps are observed for the 5% Fe doped boehmite precipitate at around 50, 150 and 351°C. For the 5% Fe doped boehmite nanofibres thermal decomposition steps are observed at 55, 120, 292 and 376°C.

As the concentration of Fe is increased the hydrothermally treated boehmite becomes a mixture of nanofibres and nanosheets. The 10% doped boehmite precipitate shows three decomposition steps at 139 to 179, 250 and 304 to 367°C. The hydrothermally treated boehmite shows three peaks at 230, 295 and 376°C. One possible assignment of these peaks is to (a) first decomposition step to goethite, (b) the decomposition of the surfactant and the third decomposition step to boehmite nanosheets. For the 20% Fe loaded boehmite the DTG patterns are similar to those of the 10% Fe doped sample. For the 20% Fe loaded boehmite nanomaterials a broad thermal decomposition is observed from 200 to 400°C with a maximum at 380°C.

Conclusions

Fe doped boehmite nanofibres 250 nm in length have been prepared at 120°C using soft chemical hydrothermal methodology using PEO as a surfactant directing agent. Fibres or needles were formed at low Fe doped samples. With the increasing iron content nanosheets are formed. Nanotubes were formed when added Fe content is increased to 20%.

Thermal analysis shows the non-treated boehmite decomposes in three steps at around 50, 150, 318 and at 397°C. The boehmite nanofibres thermally decompose at 50, 247, 312 and 403°C (Table 1). The first decomposition step is attributed to the loss of adsorbed water, the second to the loss of interstitial water and the third step to the dehydroxylation of the boehmite. In general the Fe doped boehmite nanofibres thermally decompose at higher temperatures than undoped boehmite. This is observed for both the loss of interstitial water and the dehydroxylation. For the Fe doped boehmite with Fe concentration above 5%, the thermal decomposition is of a mixed system consisting of both boehmite nanofibres and boehmite nanosheets.

Acknowledgements

The financial and infra-structure support of the Queensland University of Technology Inorganic Materials Research Program of the School of Physical and Chemical Sciences is gratefully acknowledged. The Australian Research Council (ARC) is thanked for funding the Thermal Analysis facility through a LIEF grant. One of the authors (YZ) is thankful for a Queensland University of Technology international doctoral scholarship (QIDS).

References

1 J. H. Fendler and F. C. Meldrum, Adv. Mater. (Weinheim, Germany), 7 (1995) 607.
2 B. B. Lakshmi, C. J. Patrissi and C. R. Martin, Chem. Mater., 9 (1997) 2544.
3 Y. Sun and Y. Xia, Nature, 298 (2002) 2176.
4 M. S. Gudiksen, L. J. Lauhon, J. Wang, D. C. Smith and C. M. Lieber, Nature, 415 (2002) 617.
5 J.-L. Le Loarer, H. Nussbaum and D. Bortzmeyer, (Rhodia Chimie, Fr.). Application: WO, 1998, p. 44.
6 V. S. Burkat, V. S. Dudorova, V. S. Smola and T. S. Chagina, Light Metals (Warrendale, PA, United States), (1985) 1443.
7 C. Nedez, J.-P. Boitiaux, C. J. Cameron and B. Didillon, Langmuir, 12 (1996) 3927.
8 Y. Chen, L. Jin and Y. Xie, J. Sol-Gel Sci. Technol., 13 (1998) 735.
9 D. S. Xue, Y. L. Huang, Y. Ma, P. H. Zhou, Z. P. Niu, F. S. Li, R. Job and W. R. Fahrner, J. Mater. Sci. Lett., 22 (2003) 1817.
10 A. P. Philipse, A.-M. Nechifor and C. Patmamanoharan, Langmuir, 10 (1994) 4451.
11 K. Okada, A. Tanaka, S. Hayashi, K. Daimon and N. Otsuka, J. Mater. Res., 9 (1994) 1709.
12 S. Ananthakumar, V. Raja and K. G. K. Warrier, Mater. Lett., 43 (2000) 174.
13 C. Kaya, J. Y. He, X. Gu and E. G. Butler, Microporous Mesoporous Mater., 54 (2002) 37.
14 J. Bugosh, J. Phys. Chem., 65 (1961) 1789.
15 M. P. B. Van Bruggen, Langmuir, 14 (1998) 2245.
16 D. Kuang, Y. Fang, H. Liu, C. Frommen and D. Fenske, J. Mater. Chem., 13 (2003) 660.
17 H. Y. Zhu, D. Y. Song, Y. Q. Bai, S. P. Ringer, Z. Gao, Y. X. Xi, W. Martens, J. D. Riches and R. L. Frost, J. Phys. Chem. B, 108 (2004) 4245.
18 H. Y. Zhu, J. D. Riches and J. C. Barry, Chem. Mater., 14 (2002) 2086.
19 L. Wood and J. Lindley, (Imperial Chemical Industries Ltd., UK), Application: EP EP, 1980, p. 21.
20 W. Teunissen, A. A. Bol and J. W. Geus, Catal. Today, 48 (1999) 329.
21 J. M. Bouzaid, R. L. Frost, A. W. Musumeci and W. N. Martens, J. Therm. Anal. Cal., 86 (2006) 745.
22 R. L. Frost, J. M. Bouzaid, A. W. Musumeci, J. T. Kloprogge and W. N. Martens, J. Therm. Anal. Cal., 86 (2006) 437.
23 R. L. Frost, J. Kristof, W. N. Martens, M. L. Weier and E. Horvath, J. Therm. Anal. Cal., 83 (2006) 675.
24 R. L. Frost, A. W. Musumeci, J. T. Kloprogge, M. L. Weier, M. O. Adebajo and W. Martens, J. Therm. Anal. Cal., 86 (2006) 205.
25 R. L. Frost, R.-A. Wills, J. T. Kloprogge and W. Martens, J. Therm. Anal. Cal., 84 (2006) 489.
26 R. L. Frost, R.-A. Wills, J. T. Kloprogge and W. N. Martens, J. Therm. Anal. Cal., 83 (2006) 213.
27 R. L. Frost, J. Kristof, M. L. Weier, W. N. Martens and E. Horvath, J. Therm. Anal. Cal., 79 (2005) 721.
28 R. L. Frost, M. L. Weier and W. Martens, J. Therm. Anal. Cal., 82 (2005) 115.
29 R. L. Frost, M. L. Weier and W. Martens, J. Therm. Anal. Cal., 82 (2005) 373.
30 Y.-H. Lin, M. O. Adebajo, R. L. Frost and J. T. Kloprogge, J. Therm. Anal. Cal., 81 (2005) 83.
31 H. Y. Zhu, X. P. Gao, D. Y. Song, S. P. Ringer, Y. X. Xi and R. L. Frost, Microporous Mesoporous Mater., 85 (2005) 226.
32 H. D. Ruan, R. L. Frost and J. T. Kloprogge, Spectrochim. Acta, Part A, 57A (2001) 2575.
33 H. D. Ruan, R. L. Frost, J. T. Kloprogge and L. Duong, Spectrochim. Acta, Part A, 58A (2002) 479.
34 H. D. Ruan, R. L. Frost, J. T. Kloprogge and L. Duong, Spectrochim. Acta, Part A, 58A (2002) 479.

Received: November 7, 2006
Accepted: February 22, 2007
OnlineFirst: June 28, 2007

DOI: 10.1007/s10973-006-8248-0